

Changes in the strength of the Brewer-Dobson circulation in a simple AGCM

Scott J. Eichelberger and Dennis L. Hartmann

Department of Atmospheric Sciences, University of Washington, Seattle, Washington, USA

Received 8 March 2005; revised 29 June 2005; accepted 8 July 2005; published 10 August 2005.

[1] A simple general circulation model is used to explore the response of the Brewer-Dobson circulation to warming of the tropical troposphere typically associated with greenhouse gas warming in climate models. The strength of the modeled Brewer-Dobson circulation increases in response to tropospheric tropical warming. The tropical warming causes the midlatitude baroclinicity to increase, which leads to an increase in the wave activity at synoptic and planetary scales. Increased wave propagation from the troposphere causes stronger EP flux convergence in the stratosphere. The EP flux convergence drives a stronger Brewer-Dobson circulation via downward control arguments. These results are compared to other recent GCM studies. **Citation:** Eichelberger, S. J., and D. L. Hartmann (2005), Changes in the strength of the Brewer-Dobson circulation in a simple AGCM, *Geophys. Res. Lett.*, *32*, L15807, doi:10.1029/2005GL022924.

1. Introduction

[2] Recent General Circulation Model (GCM) studies have investigated the response of the Brewer-Dobson circulation (BDC) in an environment with increased CO₂ concentrations. *Rind et al.* [1998, 2002], *Butchart and Scaife* [2001], and *Sigmond et al.* [2004] all find that the strength of the BDC increases due to CO₂ forcing. The details of each model's response are different, but results agree qualitatively. The dynamical mechanism that forces the change is, however, not yet well established. In the work by *Sigmond et al.* [2004], the tropospheric vertical wave flux decreases in their doubled CO₂ simulation. *Butchart and Scaife* [2001] and *Rind et al.* [2002], though, report that the increase in the BDC is accompanied by a larger vertical flux of wave activity from the troposphere. Thus, although CO₂ forcing causes the BDC to increase in each model, the wave response varies greatly.

[3] The temperature response of these simulations and several other models is quite consistent. In each model, increased CO₂ forcing causes deep warming of the tropics and cooling of the stratosphere. This warming leads to strengthening of meridional thermal gradients in the upper troposphere and strengthening of the subtropical jets. We hypothesize that the warming of the tropics is a critical part of the mechanism for forcing the increased BDC in the GCM's.

[4] To test this hypothesis, we use a GCM with highly simplified physics and apply idealized heating to qualitatively mimic the tropical upper tropospheric warming

typically associated with a doubled CO₂ climate. This allows us to focus on a basic dynamic mechanism responsible for driving changes in the BDC.

2. Methods

[5] Our GCM solves the dry hydrostatic primitive equations on a sphere. The model was originally developed by R. Saravanan [*Saravanan*, 1992]. Model resolution is T21 with 50 levels evenly spaced in log pressure extending from the surface to approximately 10⁻³ mb. *Polvani and Kushner* [2002] showed that results from T21 and T42 runs are consistent provided the vertical resolution is not too coarse. We verified this result with a short T42 simulation. The bottom boundary of the model is flat; thus, stationary waves are not included in our simulations. A sponge layer is applied above 10⁻¹ mb to eliminate reflections from the top boundary. Damping in the sponge layer is applied to the momentum equations using the following coefficient, $\gamma(z) = 0.25 \times [1 + \tanh(\frac{z-85}{5})]$ days⁻¹, with z given in km. Forcing in the model is applied via Newtonian relaxation of temperature to a prescribed zonally symmetric radiative equilibrium temperature field using a height dependent Newtonian cooling coefficient: $\alpha(z) = 0.05 + 0.2 \exp[-(\frac{z-50}{10})^2]$ days⁻¹. Thus the radiative damping time is 20 days⁻¹ in the troposphere and decreases to 4 days⁻¹ at ~1 mb in the stratosphere.

[6] The model is run under perpetual January conditions; therefore, the radiative equilibrium temperature field, T_{rad} , is steady in time. T_{rad} is given by

$$T_{rad}(\phi, z) = \begin{cases} T_{trop} & \text{if } z < z_T \\ w T_{strat} + (1 - w) T_{trop} & \text{if } z_T < z < z_S \\ T_{strat} & \text{if } z > z_S \end{cases}$$

where $z_T = 6$ km, $z_S = 14$ km, and $w = \frac{z - z_T}{z_S - z_T}$. T_{trop} is defined as by *Polvani and Kushner* [2002], and T_{strat} is equal to January radiative equilibrium temperatures [*Shine*, 1987].

[7] In the Winter Hemisphere upper stratosphere and mesosphere, the meridional gradient of January radiative equilibrium temperature is very large. If these temperatures were achieved, gradient wind balance implies a polar vortex with westerly winds in excess of 200 m/s. Such strong winds are not observed in the real atmosphere because gravity waves deposit easterly momentum in the mesosphere [*Holton*, 1983]. To incorporate the effect of gravity waves in our model, we apply a flow-independent force per unit mass on the zonal-mean zonal wind that is constant in time. This zonal-mean zonal wind tendency is designed to provide the drag needed to reproduce the observed distri-

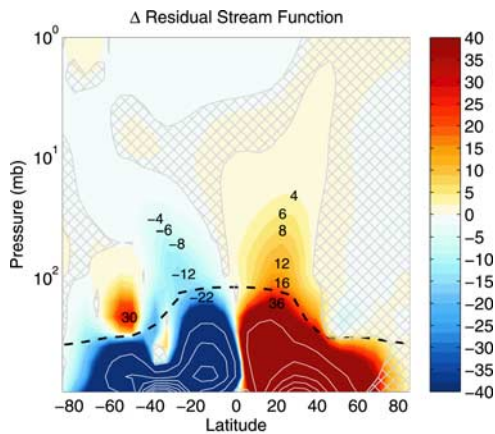


Figure 1. Time-mean difference of the residual streamfunction, kg/m/s (Heat Source–Control). White contour interval is 100; bold dashed line is the tropopause. Cross-hatched regions are not significant at the 95% level.

bution of zonal-mean zonal winds in the upper stratosphere and mesosphere in the model. (A separate model run is used to calculate the zonal-mean zonal wind tendency. In this model, damping is applied towards the initial state (Jan. climatology) with a timescale of 20 days. The zonal-mean zonal wind tendency is calculated by taking the difference of the initial and final (steady-state) zonal-mean zonal wind fields of this run and multiplying by the 20 day damping timescale.) Our zonal-mean zonal wind tendency is qualitatively similar to that shown by *Sassi et al.* [2002, Figure 1b]. Simulations using different versions of the zonal force were conducted, and the results reported below are consistent among all runs.

[8] To qualitatively simulate a doubled CO₂ climate, a zonally symmetric tropical heat source is introduced into the model,

$$Q(\phi, z) = Q_0 \exp \left[- \left(\frac{\phi - \phi_0}{\phi_w} \right)^2 \right] \sin \left(\frac{\pi z}{z_0} \right) \quad (1)$$

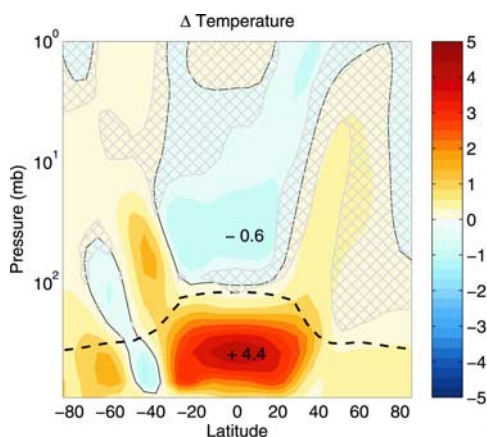


Figure 2. Time-mean difference of zonal-mean temperature (Heat Source–Control). Shading contour is 0.5 K; zero contour is black. Bold dashed line is the tropopause. Cross-hatched regions are not significant at the 95% level.

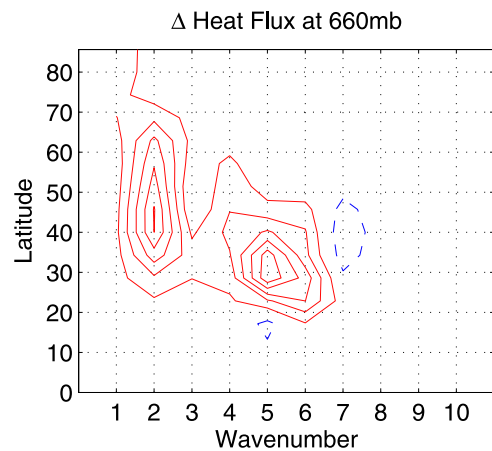


Figure 3. Wavenumber decomposition of the time-mean difference of the zonal-mean heat flux (Heat Source–Control) at 660 mb. Positive contours are solid red; negative contours are dashed blue. Contours are 0.125 ± 0.25 K m/s.

for $z \leq z_0$. Parameters are chosen to represent a tropospheric heat source centered on the equator spanning the tropics: $Q_0 = 0.5$ K/day, $\phi_0 = 0^\circ$, $\phi_w = 18^\circ$, and $z_0 = 12$ km. The amplitude of the heat source asymptotically increases to Q_0 over the first 30 days and then remains constant. Because atmospheric circulations rapidly smooth tropical temperature anomalies, results are not sensitive to ϕ_0 and ϕ_w .

[9] Initial zonal-mean temperature and zonal wind fields are set to January climatology. Variability is initiated by adding white noise to the day zero fields. Model runs are integrated for 5000 days using a 15 minute timestep. We allow 500 days for model spin-up.

3. Results

[10] The transformed Eulerian-mean (TEM) residual streamfunction, ψ , is used as a diagnostic for the BDC. Using the TEM mass continuity equation, the residual streamfunction is defined as

$$\bar{v}^* = - \frac{1}{\rho_0 \cos \phi} \frac{\partial \psi}{\partial z}, \quad \bar{w}^* = \frac{1}{\rho_0 a \cos \phi} \frac{\partial \psi}{\partial \phi}. \quad (2)$$

[11] Notation follows that of *Andrews et al.* [1987] where \bar{v}^* and \bar{w}^* are the residual mean meridional and vertical velocities, respectively. We evaluate ψ by integrating \bar{v}^* in the vertical; \bar{v}^* is calculated from gridded model output using

$$\bar{v}^* = \bar{v} - \frac{1}{\rho_0} \frac{\partial}{\partial z} \left(\rho_0 \overline{v'\theta'} / \bar{\theta}_z \right). \quad (3)$$

[12] Figure 1 shows the difference between the time-averaged residual streamfunction of the control and heat source runs. The tropopause in Figures 1 and 2 is defined by using the lower of the 3.5 PVU surface or the 380 K zonal-mean potential temperature surface. Results are only presented up to 1 mb since changes above this level are small. Cross-hatching denotes regions that are not significant at the 95% level. (The number of degrees of freedom in the significance calculation is determined using the method of

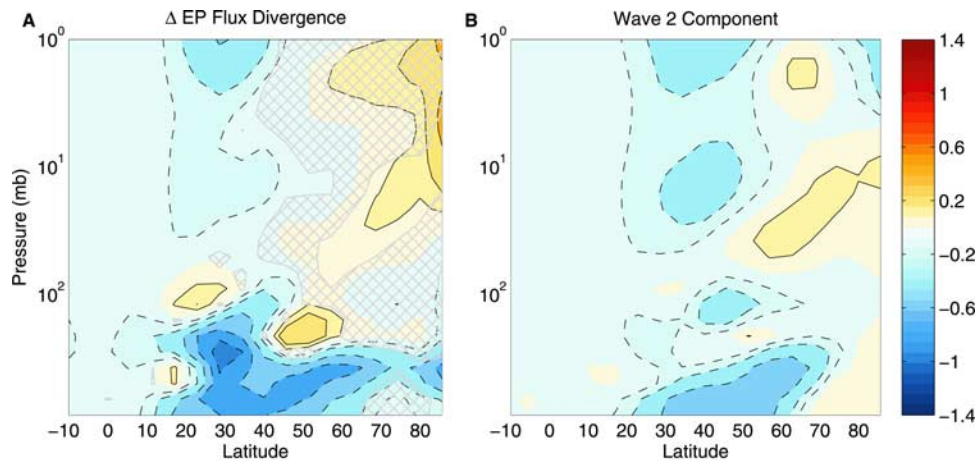


Figure 4. A) Time-mean difference of EP flux divergence (Heat Source–Control). Contour is 0.2 m/s/day with extra contours at ± 0.1 . Zero contour is omitted. Cross-hatched regions are not significant at the 95% level. B) Wavenumber 2 component of A).

Bretherton et al. [1999].) Since the control run ψ , which resembles the January-mean, is positive in the Winter Hemisphere and negative in the Summer Hemisphere, these changes indicate that the BDC is stronger in both hemispheres for the heat source run. Changes are largest in the troposphere and decrease with height because the residual streamfunction is weighted by density. ψ increases by 15% at 100 mb and 4–5% at 10 mb in the Winter Hemisphere. The change shown in Figure 1 implies a 5.0×10^8 kg/s increase in tropical upwelling. This compares well with *Butchart and Scaife* [2001], who found that the annual-mean tropical upwelling increased by 8.7×10^8 kg/s in response to increased CO_2 forcing. We will now focus on explaining a dynamical mechanism that leads to this result.

[13] The time-mean temperature difference between the heat source and control runs is shown in Figure 2. Temperatures are warmer throughout the tropical troposphere in the heat source run, with slight cooling above in the stratosphere. The most important effect of the temperature response is that the meridional temperature gradient increases in the midlatitudes for the heat source run. This causes the baroclinicity ($=g\theta_y/(\theta_0 N)$) to increase at midlatitudes. The Eady wave growth rate [*Eady*, 1949] is proportional to the baroclinicity; thus, baroclinic wave generation is expected to be greater within the region of enhanced baroclinicity. The eddy heat flux, $v'\theta'$, is proportional to the vertical flux of wave activity via the Eliassen-Palm (EP) wave flux [*Dunkerton et al.*, 1981]:

$$\mathbf{F} = \{F_{(\phi)}, F_{(z)}\}$$

$$F_{(\phi)} = -\rho_0 a \cos \phi \overline{(v'u')}$$

$$F_{(z)} = \rho_0 a \cos \phi f \overline{(v'\theta')} / \bar{\theta}_z. \quad (4)$$

[14] Figure 3 shows the wavenumber decomposition of the time-mean difference of the eddy heat flux at 660 mb between the two model runs in the Winter Hemisphere. $v'\theta'$ is generally stronger for the heat source run throughout the troposphere in the Winter Hemisphere, with differences maximized in two regions: a wavenumber 5 increase centered near 30°N and a broad wavenumber 2 increase

from 35°N to 55°N. The increase in wavenumber 5 is expected due to the stronger baroclinicity. The wavenumber 2 increase likely results from the energy cascade from smaller scales [*Tung and Orlando*, 2003] or via organization of the baroclinic eddies into planetary-scale wave packets as shown by *Scinocca and Haynes* [1998]. Although the wavenumber 5 flux is confined to the troposphere, the wavenumber 2 increase is seen at levels throughout the stratosphere (not shown). Thus, warming of the tropics causes an increase in the vertical propagation of wavenumber 2 out of the troposphere.

[15] Figure 4a displays the time-mean difference of the divergence of the EP flux between the heat source and control runs. Here we see that the EP flux convergence (negative divergence) increases throughout the troposphere and in the subtropics of the stratosphere. The region of strongest convergence in the stratosphere occurs between 20°N and 35°N, which is also where the increase in ψ is largest. Figure 4b shows that the majority of the increase in EP flux convergence in the stratosphere is due to wavenumber 2. This increase in the EP flux convergence is critical for explaining the increase in the strength of the BDC.

[16] Via the downward control principle, *Haynes et al.* [1991] showed that the residual streamfunction in the quasi-geostrophic and steady-state limit may be written as

$$\psi = \int_{z_1}^{\infty} \left[\frac{\rho_0 \cos \phi}{f} \times (\text{Force}) \right]_{\phi=\text{const.}} dz'. \quad (5)$$

[17] The ‘Force’ in Equation 5 is the total zonal force per unit mass, which is mostly due to Rossby and gravity wave breaking. In our model the effect of gravity wave breaking is a constant zonal force, and therefore does not change between the control and tropical heat source runs. The zonal force due to Rossby waves, which is equal to the divergence of the EP flux, changes when the tropical heat source is introduced (Figure 4). Thus, the vertically integrated change in the EP flux divergence causes the change in the residual streamfunction, ψ . This is seen by calculating the mass flux forced by only the resolved Rossby waves. As shown

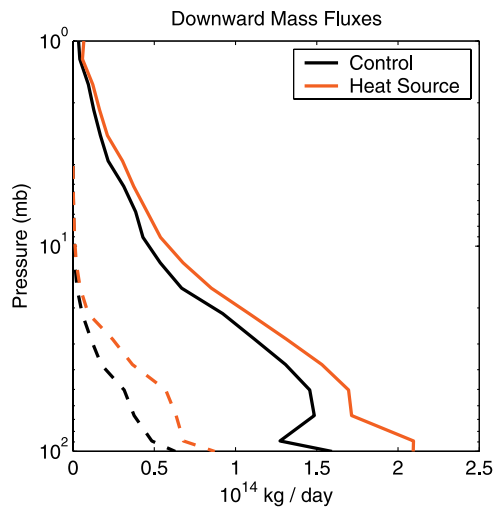


Figure 5. Hemispherically integrated downward mass flux forced by the resolved waves, kg/day. Solid lines represent the Winter Hemisphere, dashed lines the Summer Hemisphere.

by Rosenlof [1995], the hemispherically integrated downward mass flux equals $2\pi a\psi(\phi_r)$, where ϕ_r is the latitude where $|\psi|$ is a maximum, i.e. the 'turnaround' latitude. Figure 5 shows the mass flux forced by the resolved Rossby waves in the Winter Hemisphere for both model runs (solid lines). The downward mass flux is stronger, implying a stronger BDC, throughout the stratosphere for the heat source run. The mass flux difference decreases with height, which is consistent with our mechanism of a stronger tropospheric wave source driving changes in the stratospheric EP flux divergence.

[18] Although our analysis has focused on the Winter Hemisphere, where the BDC and its change are larger, the same process also occurs in the Summer Hemisphere. This is verified by examining the Summer Hemisphere downward mass fluxes shown by the dashed lines in Figure 5. The change in mass flux in the lower stratosphere is similar between the two hemispheres. An estimate of the tropical upwelling forced by the resolved waves is computed by summing the downward mass fluxes in both hemispheres. (Tropical upwelling balances extratropical downwelling.) This calculation yields tropical upwelling of 4.5×10^8 kg/s at 67 mb, which accounts for 90% of the total change in upwelling. Thus, most of the change in the BDC is forced by an increase in the EP flux convergence of the resolved waves. The majority of the increase in EP flux convergence in the stratosphere is due to wavenumber 2, which propagates up from the troposphere.

[19] The resolved mass fluxes at 90 mb in Figure 5 are approximately half the magnitude of those calculated by Alexander and Rosenlof [2003] using the UK Met Office's assimilated data set. This is not surprising since our model does not include stationary waves.

4. Conclusion

[20] Our results show that tropical tropospheric warming and associated changes in the subtropical jet structure associated with CO₂ warming can lead to strengthening of

the BDC. In agreement with Butchart and Scaife [2001] and Rind *et al.* [2002], the BDC increases because of an increased wave flux out of the troposphere. We further show that the region of enhanced tropospheric wave flux is coincident with a region of increased baroclinicity. The baroclinicity increases due to a stronger meridional temperature gradient that is driven by tropical warming. This is consistent with our hypothesis that tropical warming is critical to explaining the response of the BDC.

[21] The temperature response in the work by Sigmond *et al.* [2004] is also consistent with an increased meridional temperature gradient. Despite this, they do not show an increase in tropospheric wave activity. This suggests that the basic dynamical mechanism described here may be masked by other processes and/or parameterizations in their simulations.

[22] Although we have shown the BDC can increase without stationary waves, it is of interest to investigate the effect of stationary waves on our results. Additional shorter simulations were performed that included a 1000 m sinusoidal wavenumber 1 mountain centered at 45°N in order to excite stationary waves. The downward mass fluxes are larger in these simulations (a result of increased EP flux convergence by stationary waves), but preliminary results indicate that the change caused by tropical warming is quite similar. This provides support for our assertion that the BDC in the stratosphere increases in response to baroclinically forced planetary-scale waves, which propagate upward from the troposphere into the stratosphere. However, further work and longer model runs are needed to verify these results.

[23] All results were obtained from perpetual January simulations. Adding a seasonal cycle to our model would generate greater variability in the winter stratosphere, which might reduce the significance of our results. The mechanism described here, though, does not require coherent changes in the polar winter stratosphere (where variability would be greatest). In addition, the baroclinic wave response to the increased temperature gradient is fairly rapid. Therefore, we feel that the mechanism would operate similarly in a model with a seasonal cycle. Moreover, the GCM used by Butchart and Scaife [2001] included a seasonal cycle, and they found tropical upwelling increased in each season in response to CO₂ forcing.

[24] **Acknowledgments.** The authors would like to thank Stephen Griffiths and Stefan Fueglistaler for their many suggestions and helpful comments; Dave Ortland for sharing the model; and Keith Shine for providing the T_{strat} data. This work was supported by the Climate Dynamics Program of the National Science Foundation under grant number ATM-0409075 and NASA grant 6524 Aura/HIRDLS.

References

- Alexander, M. J., and K. H. Rosenlof (2003), Gravity-wave forcing in the stratosphere: Observational constraints from the upper atmosphere research satellite and implications for parameterization in global models, *J. Geophys. Res.*, *108*(D19), 4597, doi:10.1029/2003JD003373.
- Andrews, D. G., J. R. Holton, and C. B. Leovy (1987), *Middle Atmosphere Dynamics*, 489 pp., Elsevier, New York.
- Bretherton, C. S., M. Widmann, V. P. Dymnikov, J. M. Wallace, and I. Bladé (1999), The effective number of spatial degrees of freedom of a time-varying field, *J. Clim.*, *12*, 1990–2009.
- Butchart, N., and A. A. Scaife (2001), Removal of chlorofluorocarbons by increased mass exchange between the stratosphere and troposphere in a changing climate, *Nature*, *410*, 799–802.

- Dunkerton, T., C.-P. F. Hsu, and M. E. McIntyre (1981), Some Eulerian and Lagrangian diagnostics for a model stratospheric warming, *J. Atmos. Sci.*, *38*, 819–843.
- Eady, E. (1949), Long waves and cyclone waves, *Tellus*, *1*, 33–52.
- Haynes, P. H., C. J. Marks, M. E. McIntyre, T. G. Shepherd, and K. P. Shine (1991), On the “downward control” of extratropical diabatic circulations by eddy-induced mean zonal flows, *J. Atmos. Sci.*, *48*, 651–678.
- Holton, J. R. (1983), The influence of gravity wave breaking on the general circulation of the middle atmosphere, *J. Atmos. Sci.*, *40*, 2497–2507.
- Polvani, L. M., and P. J. Kushner (2002), Tropospheric response to stratospheric perturbations in a relatively simple general circulation model, *Geophys. Res. Lett.*, *29*(7), 1114, doi:10.1029/2001GL014284.
- Rind, D., D. Shindell, P. Lonergan, and N. K. Balachandran (1998), Climate change and the middle atmosphere. Part III: The double CO₂ climate revisited, *J. Clim.*, *11*, 876–894.
- Rind, D., P. Lonergan, N. K. Balachandran, and D. Shindell (2002), 2×CO₂ and solar variability influences on the troposphere through wave-mean flow interactions, *J. Meteorol. Soc. Jpn.*, *80*, 863–876.
- Rosenlof, K. H. (1995), Seasonal cycle of the residual mean meridional circulation in the stratosphere, *J. Geophys. Res.*, *100*, 5173–5191.
- Saravanan, R. (1992), A mechanistic spectral primitive equation model using pressure coordinates, technical report, Dep. of Appl. Math. and Theor. Phys., Univ. of Cambridge, Cambridge, U. K.
- Sassi, F., R. R. Garcia, B. A. Boville, and H. Liu (2002), On temperature inversions and the mesospheric surf zone, *J. Geophys. Res.*, *107*(D19), 4380, doi:10.1029/2001JD001525.
- Scinocca, J., and P. Haynes (1998), Dynamical forcing of stratospheric planetary waves by tropospheric baroclinic eddies, *J. Atmos. Sci.*, *55*, 2361–2392.
- Shine, K. P. (1987), The middle atmosphere in the absence of dynamic heat fluxes, *Q. J. R. Meteorol. Soc.*, *113*, 603–633.
- Sigmond, M., P. C. Siegmund, E. Manzini, and H. Kelder (2004), A simulation of the separate effects of middle-atmospheric and tropospheric CO₂ doubling, *J. Clim.*, *17*, 2352–2367.
- Tung, K. K., and W. W. Orlando (2003), The k^{-3} and $k^{-5/3}$ energy spectrum of atmospheric turbulence: Quasigeostrophic two level model simulation, *J. Atmos. Sci.*, *60*, 824–835.

S. J. Eichelberger and D. L. Hartmann, Department of Atmospheric Sciences, University of Washington, Box 351640, Seattle, WA 98195, USA. (seich@atmos.washington.edu)